APL Materials

Antiferromagnetic domain wall creep driven by magnetoelectric effect

Cite as: APL Mater. **6**, 121104 (2018); https://doi.org/10.1063/1.5053928
Submitted: 27 August 2018 • Accepted: 27 November 2018 • Published Online: 13 December 2018

Yu Shiratsuchi, Hiroaki Yoshida, Yoshinori Kotani, et al.

Antiferromagnetic domain wall creep driven by magnetoelectric effect

Yu Shiratsuchi,[1,a] Hiroaki Yoshida,[1] Yoshinori Kotani,[2] Kentaro Toyoki,[2] Thi Van Anh Nguyen,[1] Tetsuya Nakamura,[2] and Ryoichi Nakatani[1]
[1]*Department of Materials Science and Engineering, Graduate School of Engineering, Osaka University, 2-1 Yamadaoka, Suita, Osaka 5650871, Japan*
[2]*Japan Synchrotron Radiation Research Institute (JASRI)/SPring-8, 1-1-1, Kouto, Sayo, Hyogo 6796198, Japan*

(Received 27 August 2018; accepted 27 November 2018; published online 13 December 2018)

We observed the magnetoelectric induced domain wall propagation in a Pt/Co/Au/Cr_2O_3/Pt stacked thin film based on magnetic domain observations using scanning soft X-ray magnetic circular dichroism microscopy. The antiferromagnetic (Cr_2O_3) domain wall velocity was estimated by a quasi-static approach using a pulsed voltage. At a pulse voltage amplitude of −12 V, corresponding to an electric field of -8.0×10^2 kV/cm, the domain wall velocity was very low, at 0.3 m/s. The domain wall velocity increased with increasing voltage amplitude, reaching 22 m/s at −20 V (-1.3×10^3 kV/cm). The change in the domain wall velocity with the applied voltage amplitude indicates the creep motion of the domain wall. Using a phenomenological model, we estimated the domain wall depinning energy, and found that the bulk and interface terms of the magnetic anisotropy affect the effective magnetic field to the same degree, suggesting that the magnetic domain wall motion may be controllable by the antiferromagnetic layer thickness.
https://doi.org/10.1063/1.5053928

Magnetic domain wall (DW) dynamics have recently attracted considerable attention because the DW propagation often dominates the magnetization reversal process. In the DW devices, the DW velocity limits the processing speed of the device. Research has been carried out on magnetic-field,[1–3] current,[4,5] and voltage[6] induced DW motion in ferromagnetic (FM) metals[1–4,6] and diluted magnetic semiconductors.[5] By contrast, while the DW dynamics of antiferromagnetic (AFM) materials have been theoretically investigated,[7] experimental approaches are proving challenging although an experimental trial into current-induced manipulation of AFM spins has recently been initiated.[8] In current-induced FM DW dynamics, the DW propagation direction can be determined by the current flow. However, the alternatingly oriented AFM moments cancel the spin torque from the spin-polarized current, which complicates electrical detection of the AFM DWs. Furthermore, while direct observation of the magnetic domain pattern is effective, it is non-trivial to visualize AFM domains in a similar way to FM domains (for example, based on the magneto-optic Kerr effect) because AFM materials possesses no finite net magnetization.

X-ray magnetic linear dichroism (XMLD) is a powerful tool for detecting AFM spins, and it has been utilized to image AFM domains.[9,10] However, since the XMLD intensity is proportional to $\cos^2\theta$, where θ represents the angle between the AFM spin and the X-ray incident direction, the neighboring domains with collinear spins are not distinguishable, i.e., anti-phase boundaries. This is problematic for the perpendicular spin system used for modern spintronic devices. X-ray magnetic circular dichroism (XMCD), which has an intensity proportional to $\cos\theta$, resolves this problem. Nevertheless, difficulties transpire in detecting the weak XMCD signal from the interface/surface of the AFM moments since it is generated by only the tiny amount of uncompensated AFM moments.[11–13]

[a]Author to whom correspondence should be addressed: shiratsuchi@mat.eng.osaka-u.ac.jp

Another difficulty in detecting the AFM DW motion lies in driving the AFM DW propagation. The magnetic moments are fully compensated in AFM materials, and the demagnetization energy is very low. Even when a high magnetic field of several tens of kOe is applied, the spin-flop phase where the AFM moments are canted is excited; DW motion is not involved.

Previously, we showed that the uncompensated interfacial AFM (Cr) spins in a Pt/Co/Au/Cr_2O_3/Pt stacked film system, which exhibited perpendicular exchange anisotropy, could be detected by XMCD.[13] Furthermore, we demonstrated that the FM domain pattern traced that of the AFM domain owing to the strong interfacial exchange coupling.[14] In particular, when the exchange bias field exceeded the coercivity, the FM and AFM domains were coupled at remanence state.[15] Furthermore, in this system, finite magnetization could be induced in the AFM layer by applying an electric field, owing to the magnetoelectric (ME) effect of AFM Cr_2O_3.[16–18] As the electric-field-induced magnetization gained Zeeman energy from the magnetic field, the AFM DWs could be propagated by the simultaneous application of magnetic and electric fields.[19–22] Based on this mechanism, the ME-induced switching of perpendicular exchange bias polarity has been reported,[21–24] and recently, we successfully observed that the above switching process is mediated by AFM DW propagation.[15] Regarding the above techniques, we herein investigate the AFM DW dynamics of the Pt/Co/Au/Cr_2O_3/Pt stacked film.

The Pt(1.5 nm)/Co(0.4 nm)/Au(1.0 nm)/Cr_2O_3(150 nm)/Pt(20 nm) film prepared on an α-Al_2O_3(0001) substrate was used as a sample. Details of the fabrication methods and structural information can be found in our previous paper.[25] The fabricated film exhibits perpendicular magnetic anisotropy, as confirmed by the magnetization curves; the saturation magnetization M_S is about 1600 emu/cc, and the effective magnetic anisotropy energy density K_{eff} is 6.0×10^6 ergs/cc. A high M_S is seen in comparison with bulk Co (1410 emu/cc) because, although M_S is estimated using only the Co thickness, Pt and Au are also spin-polarized.[25–27]

The fabricated film was patterned into a Hall device shown in Fig. 1 by using photolithography, Ar ion milling, and lift-off processes. The width and the length of the device were 10 μm and 50 μm, respectively. Based on anomalous Hall effect (AHE) measurements, we confirmed the occurrence of ME-induced switching of the perpendicular exchange bias.[15] Typical AHE loops exhibiting the positive and negative exchange bias are shown in Fig. 2. From the AHE loops, in addition to a sharp magnetization reversal and perpendicular exchange bias field ~600 Oe higher than the coercivity (<50 Oe), the switching of the perpendicular exchange bias was confirmed. For the fabricated Hall device, magnetic domain observations were carried out using the scanning XMCD microscope at BL25SU, SPring-8. This instrument allows the magnetic domain to be imaged by the spatial distribution of the XMCD intensity, which is obtained from the difference in soft X-ray absorption intensities for positive and negative helicities. The absorption signal was collected by the total electron yield (TEY) method. Details of the observation system have been given previously.[14,28] The photon energy of the incident soft X-ray was 778.6 eV, Co L_3 edge; that is, the FM Co domains, which trace the AFM Cr_2O_3 domains, were observed.[14,15]

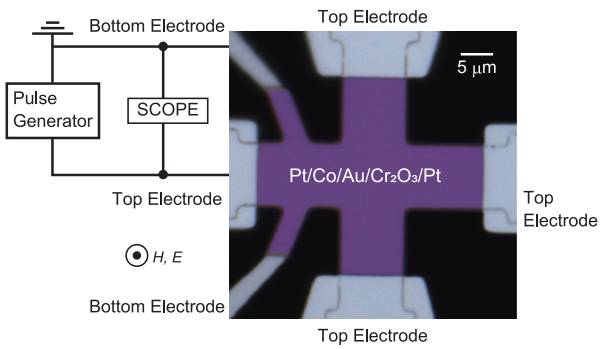

FIG. 1. Optical microscope image of the fabricated device with the equivalent circuit for the scanning XMCD microscopic imaging by the TEY method.

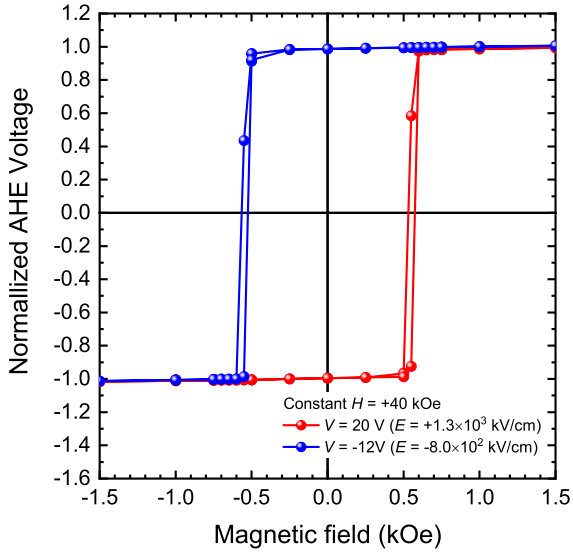

FIG. 2. AHE loops exhibiting the positive and the negative exchange bias. The positive and the negative exchange-biased state were defined by the simultaneous applications of H and $V(E)$. Red curve represents the AHE loops after the simultaneous application of H = +40 kOe and V = +20 V ($E = 1.3 \times 10^3$ kV/cm), and blue one represents the curve after the simultaneous application of H = +40 kOe and $V = -12$ V ($E = -8.0 \times 10^2$ kV/cm), respectively.

The DW velocity v was determined using the quasi-static technique, by the temperature, magnetic-field, and voltage (electric-field) sequences shown in Fig. 3. Hereafter, the positive direction of the electric and magnetic fields is defined as the direction from the bottom electrode (Pt buffer layer) to the top electrode. The process was as follows: (1) The sample was cooled from above room temperature (310 K) to the measurement temperature (285 K) under a magnetic field of +6 kOe. This defined the initial state as a negative exchange-biased state, in which the uncompensated interfacial

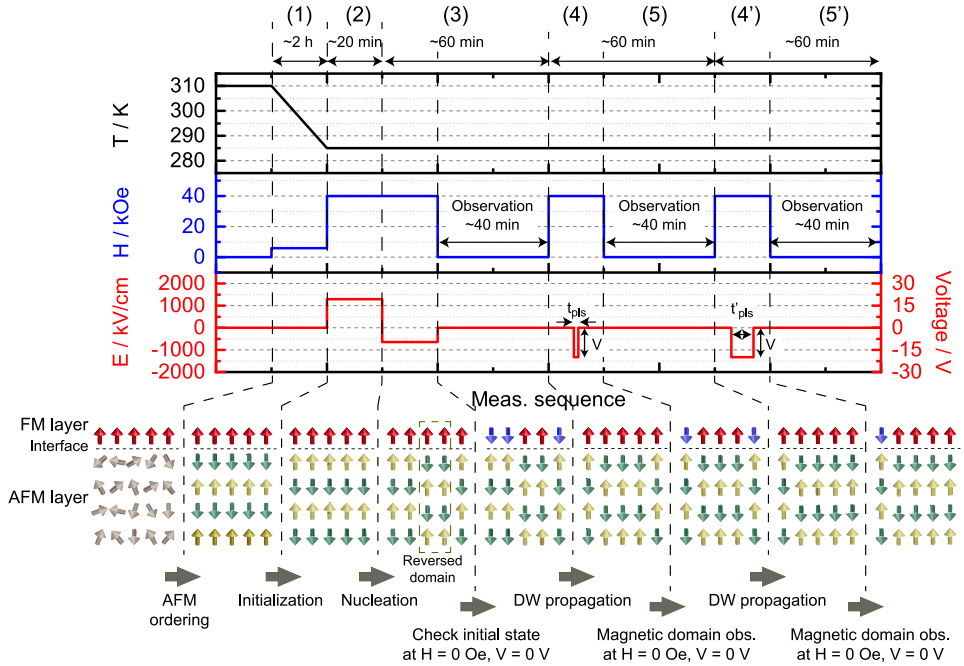

FIG. 3. Temperature, magnetic field, and voltage (electric field) sequences adopted in this paper to investigate the ME-induced DW motion. At the bottom, the assumed spin alignments at each stage are also given.

Cr spins were directed downward owing to the AFM interfacial exchange coupling between Co and Cr.[13] After stabilizing the sample temperature, (2) a constant magnetic field H of +40 kOe and a voltage V (giving an electric field E) of +19.5 V ($+1.3 \times 10^3$ kV/cm) were simultaneously applied. This process was adopted to confirm the ME effect of the device under actual use conditions; thus, the film was switched to the fully positive exchange-biased state where the interfacial uncompensated Cr spins were upward. (3) H = +40 kOe and $E = -6.4 \times 10^2$ kV/cm (−9.6 V) were applied simultaneously to nucleate the reversed AFM domain. The partially reversed state after this process, with the typical magnetic domain pattern shown in Fig. 5(a), was defined as the initial state for the AFM DW propagation. (4) Starting from the partially reversed state, H = +40 kOe and the pulse $V(E)$ were simultaneously applied. (5) After setting H = 0 kOe and V = 0 V (E = 0 kV/cm), i.e., the remanent state, the magnetic domain was imaged. Steps (4) and (5) were repeated by changing t_{pls} with the fixed pulse amplitude to induce successive DW displacement. When the amplitude of the pulse E was changed, the magnetic state was initialized again by returning to step (2) and then proceeded the successive steps. The amplitude and width of the pulse voltage (electric field) varied in the range of −9.4 V (-6.3×10^2 kV/cm) to −20 V (-1.3×10^3 kV/cm) and 30 ns–500 ms, respectively. We should note that the magnetic domain pattern at the remanent state was not changed by applying H = +40 kOe alone. Thus, the induced change in the magnetic domain pattern was driven by the simultaneous application of H and $V(E)$, agreeing with previous reports.[20–22,24,29] This ensures that the observed change in the magnetic domain pattern is caused by the ME-induced AFM DW motion.[15]

The DW displacement l was calculated from the difference of two magnetic domain images collected at steps (4) and (5), i.e., before and after applying H and each pulse $V(E)$. As an example, in the inset of Fig. 4(a), the case of H = +40 kOe and V = −20 V with t_{pulse} = 100 ns is presented, i.e., the difference image of two images shown in Figs. 5(d) and 5(e). The bright (yellow) regions in the difference image represent the DW propagated region. The DW propagation l was defined as the distance between the opposite edges of this bright (yellow) regime: the minimum distance from each pixel along the DW of the last image [the image before applying H and pulse $V(E)$]. Since the DW edge is not smooth, the l values measured from each pixel are not same, and resultantly, we can obtain the distribution of l as shown in Fig. 4(a). On analyzing l, (a) the newly nucleated region, (b) when the DW reached the edge of the Hall device, this region, (c) the coalesced region of the differently originated DW, which are indicated by circle in the inset of Fig. 4(a) were not counted. The change of mean l with t_{pls} is almost linear indicating that v is almost same for the different t_{pls}

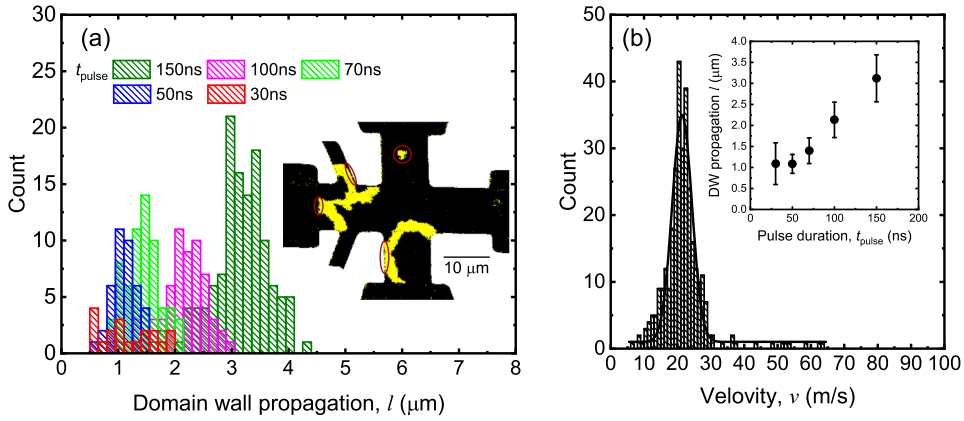

FIG. 4. Estimation method of the domain wall displacement l. In this figure, as an example, the results for the case of amplitude of pulse voltage −20 V are shown. (a) Distribution of domain wall displacement l collected after applying t_{pls} = 30 ns (red), 50 ns (blue), 70 ns (light green), 100 ns (purple), and 150 ns (dark green). The inset shows the example of difference image of the magnetic domain pattern after applying H = +40 kOe and V = −20 V with t_{pls} = 100 ns, i.e., the difference image of Figs. 5(d) and 5(e). Red circles in the inset represent the un-counted region to calculate l. (b) Distribution of domain wall velocity v collected using the distribution of l for the different t_{pls}. The inset shows the relationship between l and t_{pls} showing the linear relationship.

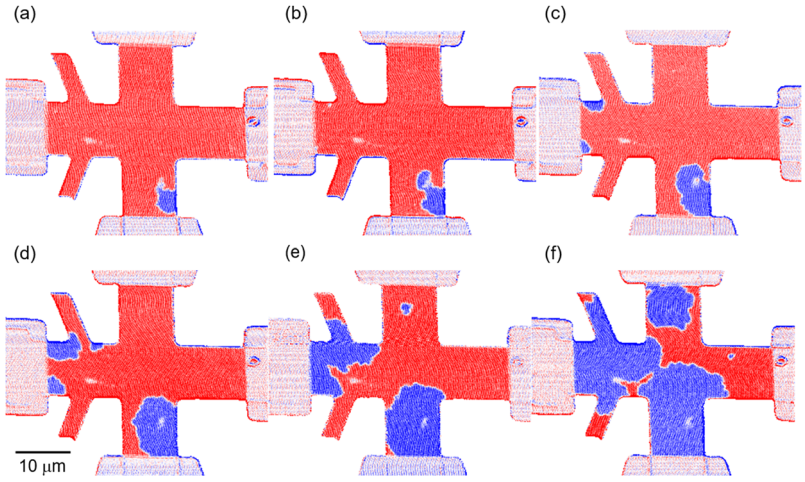

FIG. 5. Change in magnetic domain pattern with the pulse duration for the pulse amplitude of −20 V (-1.3×10^3 kV/cm): (a) initial state, and after applying H (+40 kOe) and pulse V with t_{pls} of (b) 30 ns, (c) 50 ns, (d) 70 ns, (e) 100 ns, and (f) 150 ns.

as long as the amplitude of pulse voltage was fixed. Thus, we collected the distribution of v for the certain pulse amplitude by combining the distributions of v ($=l/t_{pls}$) for the different t_{pls} [Fig. 4(b)]. From the distribution of v, the mean v and error were obtained as the peak and the standard deviation, respectively. One may wonder that the initial state defined at step (2) was not exactly same for all measurements. Since we analyzed l using the difference of two images before and after applying each pulse E, the initial state does not affect the determination of l and v.

Figures 5(b)–5(f) show the magnetic domain pattern at the remanent state after applying the various t_{pls} with a fixed pulse amplitude at −20 V (-1.3×10^3 kV/cm). The substrate regions were trimmed from the images because no TEY signal was detectable from them. Blue and red regions in the patterns correspond to the up and down Co spins, which exhibit the negative and the positive exchange bias, respectively. By the initializing process in step (2), the reversed domain (shown by the blue region) was nucleated [Fig. 5(a)]. With increasing pulse width, the reversed domain expands, meaning that the negative exchange-biased region grows. This is consistent with previous reports[20–22,24,29] although it should be noted that the applied H and E field direction is opposite and the EH product is negative. Analyzing v by the method shown in Fig. 4 yields v at −20 V (-1.3×10^3 kV/cm) as 22 ± 3 m/s. The change in v with the pulse amplitude is shown in Fig. 6. The v–$V(E)$ relationship is non-linear; v exponentially increases in the range of −12 to −16 V, which is characteristic of the creep motion of DW.[30–33] According to the ME-induced switching measurements using DC voltage for the same sample (but using a different Hall device), the DC threshold voltage to switch the exchange bias polarity was −11.7 V.[15] The creep motion of the AFM DW near the DC threshold voltage agrees with our previous report on the switching time estimation of the exchange bias polarity.[24] It has been reported that the shape of DWs is rough in the creep regime and becomes smooth in the flow regime.[32] The magnetic domain patterns after DW propagation at applied pulse amplitudes of −14 V and −20 V are inset in Fig. 6. While the DW motion is not fully in the flow regime even at −20 V as discussed below, rough DWs were observed at −14 V and smooth ones at −20 V, in agreement with the above speculation.

DW creep has previously been reported for both magnetic-field-induced motion[30–32] and current-induced motion.[5] In general, DW motion is considered under the reasonable assumption that the saturation magnetization M_S is constant. In our case, under a constant H, E was varied to induce the DW motion; the application of E induces finite magnetization via the ME effect and subsequently yields the energy gain by the Zeeman energy which acts as the driving force of DW propagation. The change in $V(E)$, i.e., the pulse amplitude, alters the amount of the induced magnetization; thus, the situation under consideration is not same as the FM case. For example, since finite magnetization is induced by the ME effect due to the imbalance of sub-lattice magnetization,

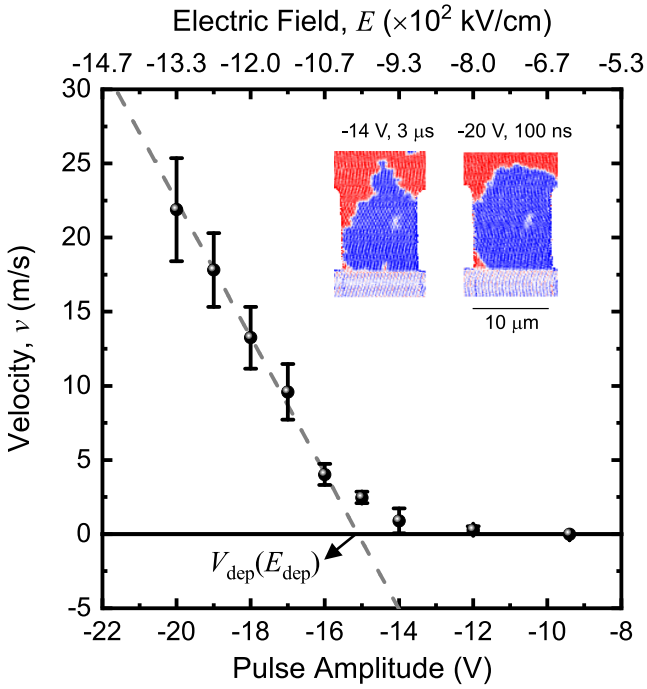

FIG. 6. Change in the DW velocity with the pulse amplitude. The insets represent magnetic domain patterns observed at the same position after applying the pulse voltage amplitude of −14 V with 3 μs width and −20 V with 70 ns width. Dashed gray line represents the linear fitting for $V = -17$ to −20 V to estimate $V_{dep}(E_{dep})$.

the application of E can change the effective Gilbert damping constant which affects v, analogous to that in ferrimagnets.[34] Besides, if the magnetic DW energy σ_{DW} is spatially changed, the effective magnetic field $H_{eff} \propto (\partial\sigma_{DW}/\partial x)/M_S$ also depends on $V(E)$. Nonetheless, as long as the driving force of the DW propagation is the Zeeman energy, the basic mechanism should be analogous to the magnetic-field-induced FM DW dynamics.[30–33] Then, v in the creep region can be expressed by

$$v(V) \propto \exp\left[-\left(\frac{U_C}{k_B T}\right)\left(\frac{V_{dep}}{V}\right)^{\mu}\right], \tag{1}$$

where U_C is related to the height of the DW pinning energy barrier, $V_{dep}(E_{dep})$ is the depinning voltage (electric field), and μ is a universal dynamic exponent. From the linear fitting in the high $V(E)$-regime shown by the dotted line in Fig. 6, i.e., −17 to −20 V (-1.1×10^3 to -1.3×10^3 kV/cm) of the v–$V(E)$ relationship, $V_{dep}(E_{dep})$ can be estimated as −15.1 V (-1.00×10^3 kV/cm).

It has been reported that μ is dependent on the dimensionalities of the DW and magnetic film and is characterized by the wandering coefficient ζ.[31,35] ζ can be determined by quantifying the edge roughness of the DWs in the creep regime: the correlation function between the displacement of the DW from the mean position, separated by a distance L is given by $\langle\langle(u[x + L] - u[x])^2\rangle\rangle \propto (L/L_C)^{2\zeta}$, where $u(x)$ is the displacement of the DW from the mean position, x is the coordinate along the direction of the DW mean orientation, and L_C is a scaling length below which the DW is flat. L_C in this work was defined by the pixel size of the magnetic domain observation, 0.15 μm. This correlation function, estimated using the DW at the applied voltage amplitude of −14 V, is shown in Fig. 7(a). The linear relationship was confirmed below $L < \sim 10$ μm, and from the slope, ζ was estimated as 0.50. The deviation from the linear relationship above $L \sim 10$ μm is probably because of the finite length of the DWs. Assuming a two-dimensional, i.e., surface interface, μ can be calculated as 2/3 through the relationship $\mu = (d - 2 + 2\zeta)/(2 - \zeta)$.[31,33] Here we briefly discuss the physical meaning of the apparent ξ. In general, $\xi = 0.5$ indicates the random walk of the DW. In this case, the deviation of from the averaged DW displacement L should be represented by a simple gaussian profile. However, as shown in Fig. 7(b), the distribution of L is not a simple gaussian but there are

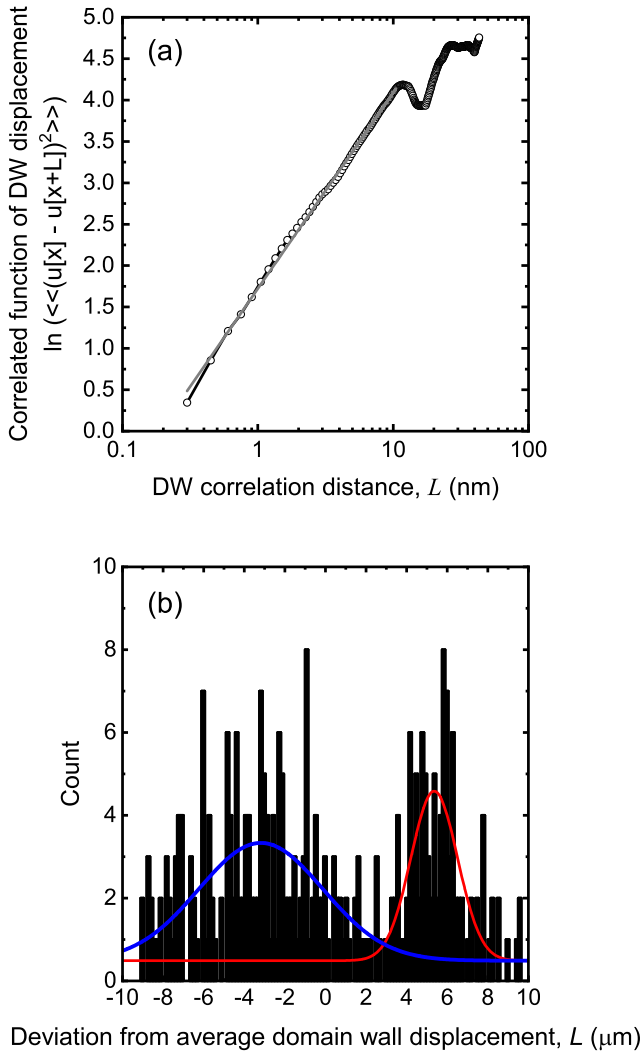

FIG. 7. (a) Correlation function of DW roughness. The gray line represents the linear fitting used to estimate ξ. (b) Distribution of the deviation from average domain wall displacement, L used to (a). Red and blue lines in (b) represent the gauusian fitting.

two peaks with the different width. At present, the physical meaning of the apparent ξ is not clear, but it may imply that the film is in some intermediate state between the ultrathin film (ξ = 2/3) and the thick film (ξ = 4/9).[31,35] It should be noted that the error of ξ could be estimated by analyzing ξ for many DWs. It is, however, difficult because the DW sufficient long for this analysis is limited because of the Hall device size.

By inserting $\mu = 2/3$ and $T = 285$ K into Eq. (1) and fitting the experimental data, U_C is estimated as $U_C = 6.1 \times 10^{-20}$ J, giving $U_C/k_BT = 15.5$. This value is similar to that for a Pt(4.5 nm)/Co(0.5–0.8 nm)/Pt(3.5 nm) trilayer (U_C/k_BT = 9–35),[32] in spite of the lower magnetic anisotropy energy density ($K_{Cr_2O_3} = 1 \times 10^4$ J/m^3 at 285 K for bulk Cr_2O_3,[36] compared with the Pt/Co/Pt trilayer[32] where $K_{eff} > 2.0 \times 10^5$ J/m^3). The similarity in U_C/k_BT can be explained by two alternative mechanisms, based on the dominant factor U_C. U_C is proportional to $K_{eff} \cdot V$ (where V is the magnetic volume of the reversed nuclei), which is expressed by $K_{eff} \cdot V = K_V \cdot V + K_{INT} \cdot S$, where K_V and K_{INT} are the bulk and interface contributions of the magnetic anisotropy energy, and S is the FM/AFM interface area of the reversed nuclei. In our case, K_{INT} is mainly caused by the interfacial exchange coupling with the FM (Pt/Co/Au) layer. According to our previous paper on the energy condition of the ME switching,[29] $K_{Cr_2O_3}$ and K_{INT} at 285 K (from the analysis of Fig. 4 in Ref. 29) are estimated as about 300 J/m^3 and 3×10^{-2} mJ/m^2, respectively. When $K_{eff} \cdot V$ is dominated by $K_{INT} \cdot S$, and assuming the diameter

of the reversed nuclei is of the same order as the DW width of Cr_2O_3 (38 nm[23]) $K_{eff} \cdot V$ becomes about 3×10^{-20} J, which is of the same order as the experimentally obtained U_C. Furthermore, our previous finding that the ME switching energy increases as the interfacial exchange coupling energy increases[37] supports the theory of significant K_{INT} contribution to K_{eff}. On the other hand, when the bulk term dominates the energy barrier, $K_{Cr_2O_3} \cdot V$ becomes about 5×10^{-20} J; this value is also of the same order as the experimentally obtained U_C. This is because the Cr_2O_3 layer thickness (150 nm) is about 20 times larger than that of the Pt(4.5 nm)/Co(0.5 nm)/Pt(3.5 nm) trilayer, and consequently, $K_{Cr_2O_3} \cdot V$ is of the same order as $K_{eff} \cdot V$ of the Pt/Co/Pt trilayer. The above arguments suggest that both the bulk and interface affect U_C to the same degree, which implies that we could control the DW creep motion by the Cr_2O_3 layer thickness.

It is also interesting that near the critical voltage of the creep motion, the absolute value of v is about 5 m/s, similar to the cases of Pt/Co/Pt[31,32] and Au/Co/Au.[30] This similarity implies the similar prefactor of Eq. (1), but the physical meaning of the prefactor is a non-trivial problem.[38] Another possibility is that the DW speed in our system is limited by the DW speed of the FM DW in the Pt/Co/Au layer. In our experiment, the high magnetic field (H = +40 kOe), sufficiently higher than the saturation field of the FM layer (see Fig. 2), was applied during the pulse $V(E)$. Namely, the FM magnetization is fixed during the H and voltage application, i.e., during the DW motion (including the nucleation) in the Cr_2O_3 layer. Hence, the influence of the DW drag in the FM layer should not be significant. However, the DW velocity is strongly influenced by the Gilbert damping parameter.[1–3] According to the theoretical prediction, the damping parameter of Cr_2O_3 is about 2×10^{-4}.[23] Our previous experiment on the dynamical switching of the exchange bias implied that the large damping parameter is >0.05,[24] similar to the Pt/Co/Pt system.[32,39] Considering this similarity, the DW velocity in our system may be limited by the enhanced damping parameter by the exchange coupling with the FM layer. For the deeper understanding of the DW motion, for example, quantitative analysis of a linear v–$V(E)$ relationship at higher values of $V(E)$ would enable us to estimate the Gilbert damping parameter. However, this is complicated by the breakdown electric field, typically around 2000 kV/cm (~30 V). Besides, according to the results shown in this paper, to increase the electric field, shorter pulses have to be applied to the Cr_2O_3 layer, i.e., below 10 ns. In this high frequency regime, the dielectric loss, i.e., the increase of ε'', would limit the DW motion in the AFM layer.

In summary, we investigated the dynamics of ME-induced DW motion in the Pt/Co/Au/Cr_2O_3/Pt stacked film based on magnetic domain observations using scanning XMCD microscopy. At a constant magnetic field of +40 kOe and an applied voltage (giving an electric field) in the range of −9.4 V (-6.3×10^2 kV/cm) to −20 V (-1.3×10^3 kV/cm), the DW velocity increases with increasing applied voltage amplitude. Below -1.0×10^3 kV/cm (−15 V), the DW velocity exponentially increases, suggesting the creep motion of the DW. From the velocity–voltage relationship, the critical voltage of the creep motion is −15.1 V. From the exponential fitting, it was found that the depinning energy of the DW was similar to that in a Pt/Co/Pt trilayer. The arguments of the depinning energy suggest that the bulk and interface terms of the magnetic anisotropy affect the DW depinning to the same degree. Therefore, we believe that the depinning energy could be controlled by the AFM layer thickness.

Magnetic domain observations using the scanning XMCD microscope were carried out with the approval of JASRI. (Proposal Nos. 2016A0079, 2016B0079, 2017A0079, and 2017B0079). This work was partly supported by the JSPS KAKENHI Grant Nos. 16H03832, 16H02389, and 18K18311, ESICMM (Elements Strategy Initiative Center for Magnetic Materials) is funded by Ministry of Education, Culture, Sports, Science and Technology, Elements Strategy Initiative Center for Magnetic Materials (MEXT) and the Photonics Advanced Research Center (PARC) at Osaka University.

[1] T. Ono, H. Miyajima, K. Shigeto, K. Mibu, N. Hosoito, and T. Shinjo, Science **284**, 468 (1999).
[2] D. Atkinson, D. A. Allwood, G. Xiong, M. D. Cooke, C. C. Faulkner, and R. P. Cowburn, Nat. Mater. **2**, 85 (2003).
[3] G. S. D. Beach, C. Nistor, C. Knutson, M. Tsoi, and J. L. Erskine, Nat. Mater. **4**, 741 (2005).
[4] L. Thomas, M. Hayashi, X. Jiang, R. Moriya, C. Rettner, and S. S. P. Parkin, Nature **443**, 197 (2006).
[5] M. Yamanouchi, J. Ieda, F. Matsukura, S. E. Barnes, S. Maekawa, and H. Ohno, Science **317**, 1726 (2007).
[6] Y. Shiota, T. Maruyama, T. Nozaki, T. Shinjo, M. Shiraishi, and Y. Suzuki, Appl. Phys. Express **2**, 063001 (2009).
[7] K. M. D. Hals, Y. Tserkovnyak, and A. Brataas, Phys. Rev. Lett. **106**, 107206 (2011).
[8] S. Fukami, C. Zhang, S. D. Gupta, A. Kurenkov, and H. Ohno, Nat. Mater. **15**, 535 (2016).
[9] F. Nolting, A. Scholl, J. Stöhr, J. W. Seo, J. Fompeyrine, H. Siegwart, J.-P. Locquet, S. Anders, J. Lüning, E. E. Fullerton, M. F. Toney, M. R. Scheinfein, and H. A. Padmore, Nature **405**, 767 (2000).

[10] K. Arai, T. Okuda, A. Tanaka, M. Kotsugi, K. Fukumoto, T. Ohkochi, F. Guo, T. Nakamura, T. Matsushita, T. Muro, M. Oura, Y. Senba, H. Ohashi, A. Kakizaki, and T. Kinoshita, Phys. Rev. B **85**, 174401 (2012).
[11] H. Ohldag, A. Scholl, F. Nolting, E. Arenholz, S. Maat, A. T. Young, M. Carey, and J. Stöhr, Phys. Rev. Lett. **91**, 017203 (2003).
[12] M. Tsunoda, T. Nakamura, M. Naka, S. Yoshitaki, C. Mitsumata, and M. Takahashi, J. Appl. Phys. **89**, 172501 (2006).
[13] Y. Shiratsuchi, H. Noutomi, H. Oikawa, T. Nakamura, M. Suzuki, T. Fujita, K. Arakawa, Y. Takechi, H. Mori, T. Kinoshita, M. Yamamoto, and R. Nakatani, Phys. Rev. Lett. **109**, 077202 (2012).
[14] Y. Shiratsuchi, Y. Kotani, S. Yoshida, Y. Yoshikawa, K. Toyoki, A. Kobane, R. Nakatani, and T. Nakamura, AIMS Mater. Sci. **2**, 484 (2015).
[15] Y. Shiratsuchi, S. Watanabe, H. Yoshida, N. Kishida, R. Nakatani, Y. Kotani, K. Toyoki, and T. Nakamura, "Observation of the magnetoelectric reversal process of the antiferromagnetic domain," Appl. Phys. Lett. (to be published).
[16] V. J. Folen, G. T. Rado, and E. W. Stalder, Phys. Rev. Lett. **6**, 607 (1961).
[17] D. N. Astrov, Sov. Phys. JETP **11**, 708 (1960).
[18] A. Iyama and T. Kimura, Phys. Rev. B **87**, 180408(R) (2013).
[19] T. J. Martin and J. C. Anderson, IEEE Trans. Magn. **2**, 446 (1966).
[20] X. He, Y. Wang, N. Wu, A. N. Caruso, E. Vescovo, K. D. Belashchenko, P. A. Dowben, and C. Binek, Nat. Mater. **9**, 579 (2010).
[21] K. Toyoki, Y. Shiratsuchi, A. Kobane, C. Mitsumata, Y. Kotani, T. Nakamura, and R. Nakatani, Appl. Phys. Lett. **106**, 162404 (2015).
[22] T. Ashida, M. Oida, N. Shimomura, T. Nozaki, T. Shibata, and M. Sahashi, Appl. Phys. Lett. **106**, 132407 (2015).
[23] K. D. Belashchenko, O. Tchernyshyov, A. A. Kovalev, and O. A. Tretiakov, Appl. Phys. Lett. **108**, 132403 (2016).
[24] T. V. A. Nguyen, Y. Shiratsuchi, and R. Nakatani, Appl. Phys. Express **10**, 083002 (2017).
[25] Y. Shiratsuchi, W. Kuroda, T. V. A. Nguyen, Y. Kotani, K. Toyoki, T. Nakamura, M. Suzuki, K. Nakamura, and R. Nakatani, J. Appl. Phys. **121**, 073902 (2017).
[26] M. Suzuki, H. Muraoka, Y. Inaba, H. Miyagawa, N. Kawamura, T. Shimatsu, H. Maruyama, N. Ishimatsu, Y. Isohama, and Y. Sonobe, Phys. Rev. B **72**, 054430 (2005).
[27] F. Wilhelm, M. Angelekeris, N. Jaouen, P. Poulopoulos, E. Th. Papaioannou, Ch. Mueller, P. Fumagalli, A. Rogalev, and N. K. Flevaris, Phys. Rev. B **69**, 220404(R) (2004).
[28] Y. Kotani, Y. Senba, K. Toyoki, D. Billington, H. Okazaki, A. Yasui, W. Ueno, H. Ohashi, S. Hirosawa, Y. Shiratsuchi, and T. Nakamura, J. Synchrotron Radiat. **25**, 1444 (2018).
[29] T. V. A. Nguyen, Y. Shiratsuchi, A. Kobane, S. Yoshida, and R. Nakatani, J. Appl. Phys. **122**, 073905 (2017).
[30] A. Kirilyuk, J. Ferré, J. Pommier, and D. Renard, J. Magn. Magn. Mater. **121**, 536 (1993).
[31] S. Lemerle, J. Ferré, C. Chappert, V. Mathet, T. Giamarchi, and P. Le Doussal, Phys. Rev. Lett. **80**, 849 (1998).
[32] P. J. Metaxas, J. P. Jamet, A. Mougin, M. Cormier, J. Ferré, V. Baltz, B. Rodmacq, B. Dieny, and R. L. Stamps, Phys. Rev. Lett. **99**, 217208 (2007).
[33] P. J. Metaxas, Solid State Phys. **62**, 75 (2010).
[34] R. Giles and M. Mansuripur, J. Magn. Soc. Jpn. **15**, 299 (1991).
[35] M. V. Fiegle'man, V. B. Geshkenbien, A. I. Larkin, and V. M. Vinokur, Phys. Rev. Lett. **63**, 2303 (1989).
[36] S. Foner, Phys. Rev. **130**, 183 (1963).
[37] K. Toyoki, Y. Shiratsuchi, A. Kobane, S. Harimoto, S. Onoue, H. Nomura, and R. Nakatani, J. Appl. Phys. **117**, 17D902 (2015).
[38] P. Chauve, T. Giamarchi, and P. Le Doussal, Phys. Rev. B **62**, 6241 (2000).
[39] S. Mizukami, E. P. Sajitha, D. Watanabe, F. Wu, T. Miyazaki, H. Naganuma, M. Oogane, and Y. Ando, Appl. Phys. Lett. **96**, 152502 (2010).